ACS Sustainable Chemistry & Engineering
pubs.acs.org/journal/ascecg

Research Article

Effective and Fast-Screening Route to Evaluate Dynamic Elastomer-Filler Network Reversibility for Sustainable Rubber Composite Design

Tian Xia, Alan M. Wemyss, Reza Salehiyan, Ellen L. Heeley, Xiao Hu, Fengzai Tang, Yuchen Sun, Darren J. Hughes, Tony McNally, and Chaoying Wan*

Cite This: https://doi.org/10.1021/acssuschemeng.3c06752 Read Online

ACCESS | Metrics & More | Article Recommendations | Supporting Information

ABSTRACT: The introduction of self-healing and reprocessability into conventional vulcanized rubbers has been recognized as a promising strategy to promote elastomer circularity. However, the reversibility and recovery of cross-linking polymer networks have often been assessed by static mechanical testing, which highly limits the understanding of the underlying microscale mechanisms. In this work, we investigated the network recovery of natural rubber (NR)/carbon black (CB) nanocomposites using Fourier transform (FT) rheology coupled with large amplitude oscillation shear (LAOS) technology across linear and nonlinear regimes (0.01−500%). The self-healing process of the rubber composite networks was monitored by using a programmed time−temperature oscillation shear measurement. The role of CB particle size in the filler network recovery was also discussed from the perspective of strain-induced crystallization of NR. Coupling FT-rheology and LAOS analysis, two distinct nonlinear enhancement behaviors beyond the linear viscoelastic regime were detected in the rubber nanocomposites, which were ascribed to the filler network disruption followed by the polymer network deformation. The relationship of the nonlinearity parameter $I_{3/1}$ as a function of strain amplitude was selected to quantify the nonlinear rheological responses, where the role of the filler and polymer on the network recovery can therefore be differentiated. This work provides an efficient method to evaluate the self-healing and reprocessability of cross-linked rubbers and offers a fast-screen route for formulation development and sustainable rubber composite design.

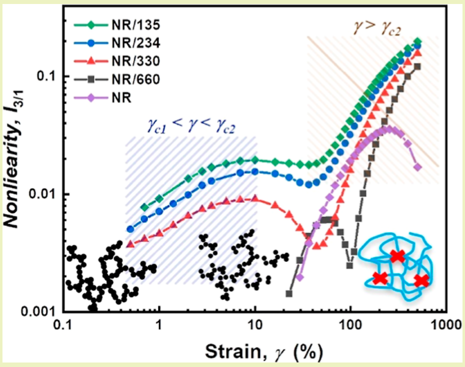

KEYWORDS: *polymer/filler network, self-healing, cross-link density, rheology*

INTRODUCTION

Thermoset polymers and vulcanized rubbers are persistent challenges for recycling due to their permanently cross-linked chemical structures that are not soluble or meltable. Great efforts have been dedicated to designing macromolecular networks for self-healing or reprocessability, which further complicates the interactions within the polymer−polymer, polymer−filler, and filler−filler networks in composites.

Understanding the behavior of complex structures in filled vulcanized rubber systems is crucial for the development of products, particularly when considering materials with reprocessing or self-healing characteristics. Such applications could include tires, seals, and gaskets, where the material is subjected to repetitive or fluctuating loads and must maintain its properties over extended periods. Therefore, a thorough understanding of the dynamic behavior of carbon black-filled natural rubber (NR/CB) systems and the effect of CB particle size during self-healing cycles can provide valuable insights into the material's performance and potential applications. In this context, dynamic oscillatory shear measurement is a valuable technique for investigating the microstructures of materials at different deformation levels. Small amplitude oscillatory shear (SAOS) testing is commonly used to determine the linear viscoelastic properties of materials, providing some information about the microstructure and morphology of the materials. However, SAOS testing is limited to the linear viscoelastic behavior of the materials, and the nonlinear responses under large deformations are not captured. Moreover, SAOS tests may result in similar linear viscoelastic responses in materials with different nonlinearities. Therefore, large amplitude oscillation shearing (LAOS) measurements are necessary for nonlinear viscoelastic characterization.

For instance, Nie et al.[1] discovered a higher sensitivity of the third harmonics to changes from the aging of NR/CB composites than was found in their linear rheological properties.

Received: October 17, 2023
Revised: November 22, 2023
Accepted: November 27, 2023

Similar higher resolution sensitivity has been reported in a series of works by Leblanc, where Fourier transform (FT)- rheology was used as the main characterization tool in filled rubber systems as opposed to conventional linear rheological methods.[2−4] The findings revealed that FT-rheology is capable of capturing the filler contribution in the NR/CB systems. Specifically, the results showed a distinctive "bump" in the FT-rheology data, which is attributed to the strong interaction between the CB filler and the rubber matrix. This interaction yields enhanced harmonics at medium strain amplitudes, providing insight into the nonlinear viscoelastic behavior of the materials.[5] In recent work, Nie et al. developed a model to describe the $I_{3/1}$ evolution in a filled rubber system.[6] It is proposed that nonlinearities arise from the deagglomeration and agglomeration of fillers below a certain critical strain, while the nonlinearities at higher strain amplitudes are the reflection of polymer chain deformation and orientations.

Accounting for the developments in LAOS tests, particularly the FT-rheology technique, it can be used as a powerful tool to investigate the effect of CB size on the nonlinear viscoelastic response of filled vulcanized rubber systems during self-healing cycles. The FT-rheology enables the investigation of the filler network and rubber entanglement (cross-link density) contributions with respect to CB particle size. Moreover, the effect of self-healing or reprocessing cycles can be studied using FT-rheology, thereby providing valuable insights into the behavior of the material under different conditions, e.g., different strains and frequencies. Therefore, FT-rheology is a valuable technique for product development, particularly in applications in which reprocessing or self-healing characteristics are required.

Self-healing behavior is an important aspect of rubber materials. A variety of reversible chemical bonds, such as disulfides,[7−9] Diels−Alder adducts,[10,11] boronic esters,[12,13] and imines,[14,15] have been introduced to rubbers and act as part of the chemical cross-links for stimuli-triggered self-healing and reprocessing.[16,17] Among them, disulfide chemistry is attractive since the exchange of disulfides and the corresponding healing process is able to occur under mild conditions.[18] For example, An et al. utilized a click-type photoinduced thiol−ene radical addition and oxidation to synthesize dual-sulfide-disulfide cross-linked networks with rapid self-healing properties at room temperature without any external stimuli.[19]

Turning vulcanized natural rubber (NR) into a self-healing material is challenging due to its nonpolar nature and low reactivity. In sulfur-based vulcanization systems, the contents of disulfide, polysulfide, and monosulfide bonds can be varied by tuning the sulfur content and the accelerator/sulfur ratios.[20] Gent and Lai[21] found that partially cured elastomers could macroscopically heal by rearranging their rubber network without deterioration of mechanical properties. Afterward, the possibility of developing self-healing NR during the cross-linking process was verified in conventional vulcanized NR formulations.[22] The underlying mechanism for self-healing was disulfide metathesis based on temperature-driven sulfur reactions. CB is an effective reinforcement filler for NR. The effects of cross-link chemistry and filler types on the self-healing of rubbers have been investigated,[23−25] which are often evaluated by the recovery efficiency of mechanical properties. There is a lack of understanding of how the microscale polymer−filler and filler−filler network impact the macroscale self-healing and reprocessabilty of the cross-linked rubbers.

In the study conducted by Khimi et al.,[26] an investigation was carried out to examine the impact of CB on the self-healing characteristics of NR. The results of their study revealed that the inclusion of CB had a detrimental effect on the efficiency of tensile strength healing. This phenomenon was attributed to the limited availability of free rubber necessary for the healing process. Essentially, the presence of CB particles imposed restrictions on the mobility and accessibility of the rubber phase required for effective self-healing, thus, impeding the healing process within the network structure. Utrera-Barrios et al.,[27] in contrast, observed an enhancement in the healing efficiencies of rubbers composed of epoxidized natural rubber and thermally reduced graphene oxide (TRGO). Their study highlighted the significant contribution of functional particles to facilitating the healing process. It was found that the introduction of TRGO led to the establishment of hydrogen bonds between its functional groups and the oxirane rings. Consequently, this interaction facilitated a notable improvement in healing efficiency, reaching 82% tensile strength and 86% elongation at break. The studies presented above suggest the important role of fillers in healing properties.

In this work, four industrial-grade CB particles were selected as reinforcement for NR. The effect of CB particle size on the polymer−filler network recovery ability was investigated and quantified by using FT-rheology under LAOS (0.01−500%), which is further correlated to the static mechanical self-healing testing. The reinforcement effect of the CB was also characterized by using time-resolved tensile testing coupled with wide-angle X-ray scattering (WAXS), from the perspectives of filler dispersion, interfacial interactions, and strain-induced crystallization (SIC) of NR. The effect of CB particle size on the linear and nonlinear dynamic properties is discussed.

EXPERIMENTAL SECTION

Materials. NR (TSR10, Africa), stearic acid (SA), zinc oxide (ZnO), and *N*-cyclohexyl-2-benzothiazolesulfenamide (CBS) were commercial products and used as received. Four industry grades of CB with particle sizes in the order N660 > N330 > N234 > N135 were compounded with NR, the structure properties of the CBs are detailed in Table 1. The CB morphology was characterized by transmission electron microscopy (TEM, Figure S1) and the primary particle sizes as detailed in Table 1. The CB dispersion in rubbers was examined by using a Zeiss Gemini scanning electron microscope with a field emission electron gun operating at 3 kV.

Table 1. Structural Properties of the Four CB Grades Used in This Study

grade	name	nitrogen absorption (m^2/g)	iodine absorption (mg/g)	DBP absorption (mL/100 g)	average particle size (nm)
N660	GPF	35	36	90	50
N330	HAF	78	82	102	29
N234	ISAF	119	120	125	25
N135	HS-SAF	139	153	140	22

Preparation and Characterization. The NR compounds were prepared using a Haake Polylab internal mixer at a rotor speed of 70 rpm using the formulation listed in Table 2, with an initial compounding temperature at 50 °C and mixed for 10 min. A lower sulfur content was used—refers to Hernández's work[20] for enhanced network mobility. The control NR sample without CB was prepared following a conventional vulcanized formulation containing a curing activator (SA/ZnO 1/5 phr). After mixing, the compounds were cured into 100 mm × 100 mm × 1 mm sheets at 150 °C and 20 MPa according to their optimum cure time t_{90} measured by using a rubber process analyzer (RPA) (Montech 3000, Germany).

Table 2. Formulations for the NR/CB Composites

ingredient	composition (phr)
NR	100
CB	40
ZnO	5
SA	1
N-cyclohexylbenzothiazole-2-sulfenamide (CBS)	0.14
sulfur (S)	0.7

The curing properties (Figure S2 and Table S1), bound rubber (Figure S3),[28] and cross-linking density (Table S2)[29] measurements were detailed in the Supporting Information.

Tensile testing was performed at 200 mm/min at room temperature, using a Shimadzu Autograph AGS-X tester, according to the ASTM-D638−14 type V. A lap-shear test was conducted to evaluate the self-healing performance of the vulcanized NR. To ensure good contact, a force of 20 N was used and self-healing was assessed at 80 °C for 2 h. The self-healing efficiency (recovery %) was quantified by the ratio of maximum stress (σ_{max}) or stroke strain (γ_{stroke}) before and after healing, $\frac{\sigma_{\text{stroke}}(\text{healed})}{\sigma_{\text{stroke}}(\text{original})}$, or $\frac{\gamma_{\text{stroke}}(\text{healed})}{\gamma_{\text{stroke}}(\text{original})}$.

Dynamic mechanical thermal analysis (DMTA) was performed on a Triton Tritec 2000 DMA instrument in tension mode. Rectangle samples with dimensions of 6 × 10 × 2 mm were tested with a temperature sweep from −80 to 100 °C and a heating rate of 3 °C/min. A fixed frequency of 1 Hz and strain of 0.5% was applied.

Dynamic shear rheological behavior was performed using an RPA analyzer (Montech 3000). LAOS was measured at a frequency of 1 Hz with strain amplitudes from 0.1 to 500% at 60 °C to quantify the nonlinear viscoelasticity. For the self-healing assessment using RPA, a dynamic program has been established including three cycles of an amplitude sweep. The compound was first cured at 150 °C for t_{90} as the curing time, and subsequently cooled to 60 °C and held for 3 min. Then the first amplitude sweep was applied in a range of 40 different strain amplitudes from 0.07 to 500%, at a frequency of 1 Hz. After this procedure, the sample was isothermally relaxed at 80 °C for network recovery. Next, the sample was cooled to 60 °C, held for 3 min, and subjected to a second amplitude sweep following the same conditions as the first one. This cycle of heating for self-repairing and subsequent cooling and testing was repeated, including a third amplitude sweep under the same conditions.

Synchrotron X-ray scattering measurements: WAXS measurements were performed on the XMaS (BM28) beamline at the European Synchrotron Radiation Facility (ESRF), France. The X-ray data was obtained using a wavelength $\lambda = 1.033$ Å and a beam spot size of 138 μm × 70 μm. 2D WAXS data was collected on a Pilatus 1 M detector which was positioned at a distance of 276 mm from the sample position (see Figure S4a,b). The detector was calibrated with LaB_6.

The dumbbell rubber samples were secured in the jaws of a Linkam TST350 tensile testing instrument with a 200 N load cell, positioned vertically to the X-ray beam. The rubber samples were drawn in the tensile tester at ambient temperature and a rate of 60 μm/s to a maximum elongation of 400% (as shown in Figure S4c). This ensured that all of the samples for SIC experiments did not fail during testing, on the basis of the tensile results shown in Figure 1a. During the draw 2D WAXS patterns were obtained at a frame rate of 1 s with a dead time then of 9 s. All WAXS data were normalized for sample thickness, transmission, and background scattering. WAXS data was analyzed using the Dawn X-ray analysis software.[30] The 2D WAXS data was reduced to 1D scattering profiles by sector averaging in 5° steps around the beam stop at a fixed radius, q.

RESULTS AND DISCUSSION

Reinforcement and Self-Healing Measured by Tensile Testing. Diene rubbers such as NR or styrene-butadiene rubber (SBR) are generally cured via accelerated sulfur vulcanization systems, including conventional vulcanization (CV), semi-efficient vulcanization (SEV), and efficient vulcanization (EV). The three curing systems differ in their sulfur content and accelerator:sulfur ratio. The CV system contains a higher sulfur content (2.0−3.5 phr) and lower accelerator:sulfur ratio (0.1−0.6) as compared to SEV and EV and generates higher amounts of poly- and disulfide bonds in the cured rubbers, therefore providing better mechanical strength and fatigue resistance, but lower thermal and reversion resistance.[31] By reducing the sulfur content in the CV system, thermally triggered self-healing behavior was observed in vulcanized NR.[20,32]

In this work, we chose a modified CV curing package with a sulfur content of 0.7 phr and an accelerator:sulfur ratio of 0.2, as a route to lowering the cross-link density and magnifying the self-healing behavior. Four types of commercial CB with particle size in the range of 22−50 nm were selected, where the size increases in the order of N135 < N234 < N330 < N660. As examined by SEM (Figure S5), the four types of CB particles were all homogeneously distributed in NR at 40 phr, with

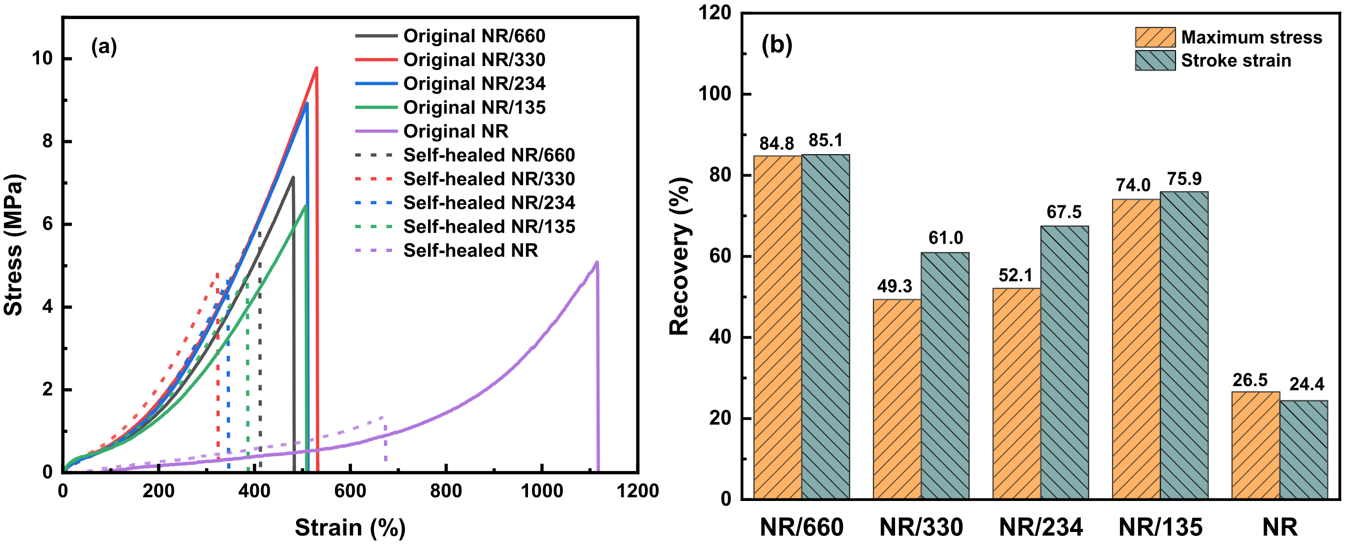

Figure 1. (a) Mechanical tensile stress−strain curves of NR/CB composites before and after self-healing; (b) Self-healing recovery of the NR/CB composites.

agglomerates being less than 1 μm. In the following, the effects of CB particle size on the filler network formation and the role of filler network recovery on the macroscopic self-healing behavior of the composites are investigated.

The self-healing performance of the cured NR/CB samples was first evaluated by tensile testing. The samples were cut into halves, then overlapped and healed at 80 °C for 2 h.[32] The tensile stress−strain results of the NR/CB composites before and after self-healing are compared in Figure 1a. The addition of the CB filler made an obvious reinforcement effect on the neat NR regardless of particle size. Among them, the N330 and N234 exhibited greater reinforcement than N660 and N135 (Figure 1a). The reason for this will be explored in the next discussion on SIC in NR. After self-healing at 80 °C for 2 h, the NR/660 showed the highest recovery in both the stress and strain (Figure 1b). Except for NR/660, the other NR/CB composites revealed an increasing recovery with the reduction of CB size from N330 to N135.

The well-dispersed CB particles also participate in interfacial interactions, and the bound rubber content was determined using a solvent-extraction method. Figure 2 shows the uncured NR/234 has the largest bound rubber content (3.85%) over the other compounds, and it also shows the highest cross-linking density (5.21×10^{-5} mol cm^{-3}) after curing (Table S2).

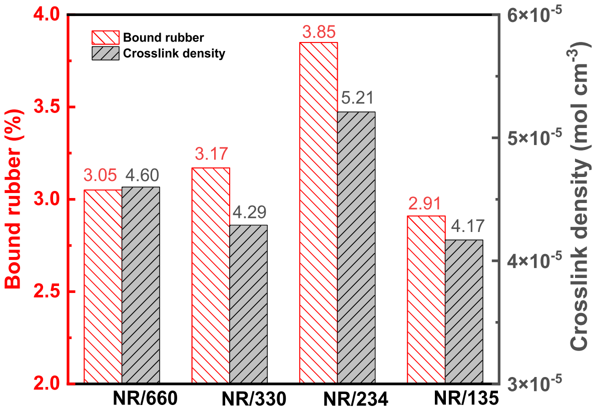

Figure 2. Bound rubber and cross-link density for NR/CB composites.

In addition, the mechanical reinforcement of NR by CB is also attributed to SIC in NR. We examined the SIC behavior of the NR/CB composites at ambient temperature using in situ tensile testing with synchrotron WAXS, Figure 3. This allows the development of the crystalline structure to be mapped on the tensile stress−strain curves; the data for the four NR/CB composites and the unfilled NR sample are shown.

As shown in Figure 3a, the addition of 40 phr CB led to an upturn of the stress in all NR/CB composites occurring at lower strain compared with the unfilled NR rubber,[33,34] confirming the increased mechanical performance of the composites. Of the NR/CB samples, the NR/330 composite shows the greatest reinforcement, followed by NR/135.

Figure 3b shows the 2D WAXS patterns of all of the NR/CB composites and unfilled NR at the final strain of 400%. Due to the positioning of the detector, the 2D patterns show only half of the overall scattering data. However, the equator of the pattern where the crystalline peaks emerge during SIC is captured with this positioning of the detector. The main crystalline peaks (as labeled) on the NR/330 WAXS pattern, are indexed as the (200), (201), and (120) which are assigned to the monoclinic unit cell where a = 12.5 Å, b = 8.9 Å, c = 8.1 Å and β = 92°, as proposed by Bunn for NR.[35] From the 2D WAXS patterns at 400%, all of the NR/CB composites show the clear development of the crystalline peaks in contrast with unfilled NR, which shows less crystalline peak development at this strain value.

In Figure 3c, the 2D WAXS patterns are plotted on the stress−strain curve for the NR/330 composite, between 100 and 400%. The onset of crystallization is seen in the NR/330 composite at around 150−200% strain. Interestingly, the onset of crystallinity in the WAXS data can be correlated with an increase in stiffness in the sample as seen in the mechanical testing.

Figure 4 shows the surface plots for equatorial scattering intensity for all NR/CB composites and the NR control sample over the 2θ region of 9−17°. The plots are shown from 0 to 400% strain. The surface plots should be considered alongside the full diffraction patterns shown in Figures 3b and c. For all NR/CB composites at higher strain, the main crystalline (200) and (120) peaks develop at 10.7 and 15.6°, respectively. Below 100% strain a broad scattering intensity centered at ∼13.5° is observed, indicating an unoriented network of amorphous rubber chains. At a strain of between 150 and 200%, the (200) and (120) oriented crystalline peaks start to develop from the SIC process, and at 400% these crystalline peaks are evident in all the NR/CB composites. For each NR/CB composite, the onset of SIC occurs under different strains. However, there is still evidence of the amorphous intensity at 400%, indicating that there are still unoriented and oriented amorphous rubber chains coexisting in the rubber network. In contrast, the unfilled rubber does not show any significant crystalline peak development until ∼350% strain, where a very weak (200) peak starts to develop via SIC. It should be noted that in previous studies, NR without filler shows the onset of SIC at higher strains of ∼400%,[36,37] so this agrees with other observations. These observations provide strong evidence that the CB filler advances the onset of the SIC process and crystalline development in the composites compared to that in the unfilled rubber system. A similar phenomenon has been observed in rubber composites with the CB filler. For example, Huneau[33] summarizes that it is well-known that the addition of CB to NR induces SIC at lower strains due to particle nucleating affects in the rubber matrix.

To quantitatively explore the onset of SIC at ∼200% strain and the final crystalline structure at 400% 1D WAXS profiles were taken of the 2D WAXS patterns. The equatorial intensity was integrated over a ±10° azimuthal range for the (200) and (120) peaks.[37,38] Figure 5a,b shows the development of the (200) and (120) peaks at 200% strain and 400% strain respectively. From the 1D WAXS profiles at 200% strain, the (200) and (120) peaks are seen in the NR/330 composite and are less developed in the other composites. In the unfilled NR sample, the peaks are not observed at 200% strain. At 400% strain, the (200) and (120) reflections are evident in all the NR/CB composites, but only the weak (200) reflection is observed in the unfilled NR sample. Therefore, SIC occurs at lower strains in the NR/CB composites compared to unfilled NR, indicating that the CB filler enhances SIC in this strain region. As mentioned previously, the positive effect of CB fillers on driving SIC has been widely recognized. However, it can be noted that there is a lack of detailed understanding of the relationship between particle properties (size/type/shape) and the nucleation process. As seen above, we observe that the N330 CB leads to the earliest onset of SIC. This shows that the SIC effect is not simply driven by particle size but rather possibly that an *optimum*

https://doi.org/10.1021/acssuschemeng.3c06752
ACS Sustainable Chem. Eng. XXXX, XXX, XXX−XXX

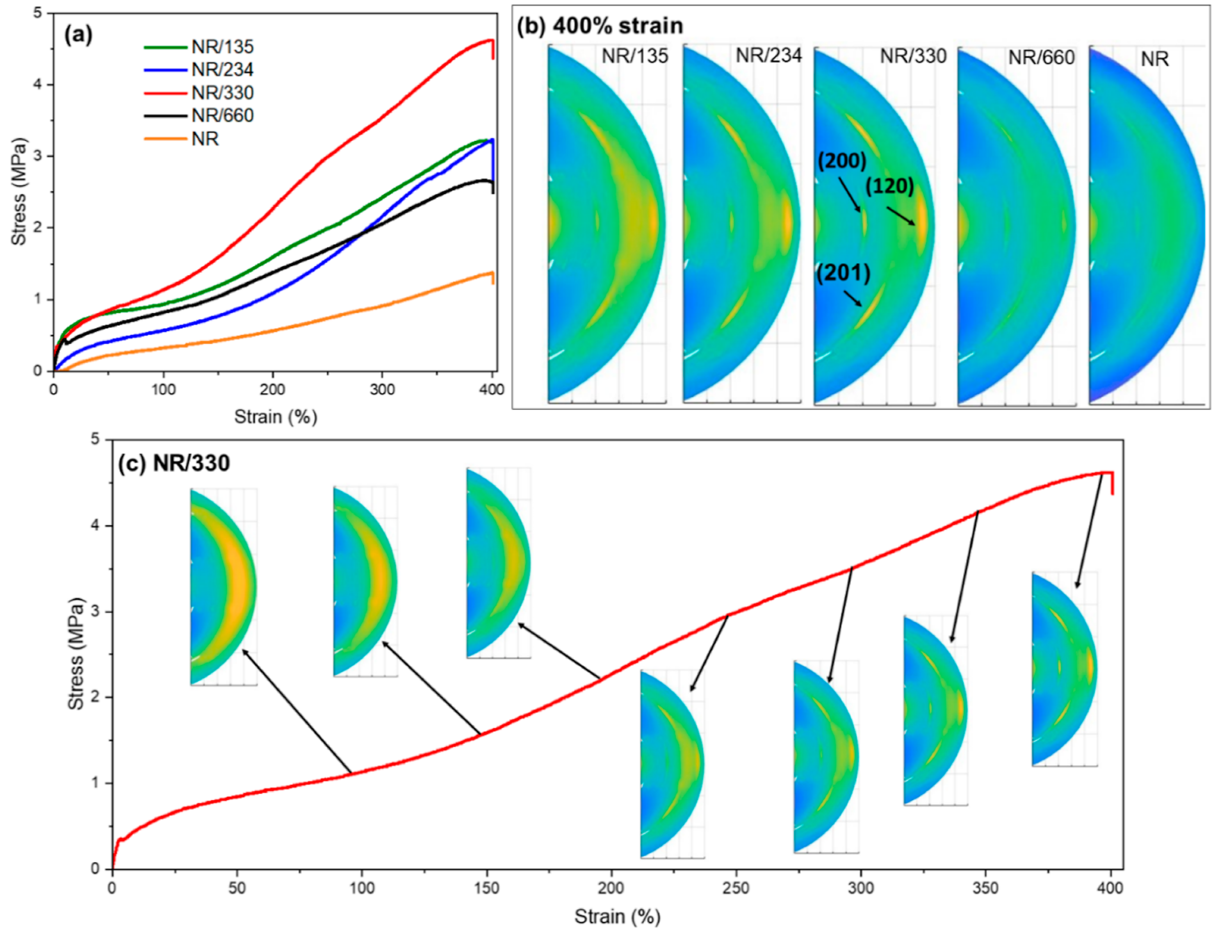

Figure 3. (a) Stress−strain curves at ambient temperature; (b) 2D WAXS patterns of all samples at 400% strain (the draw direction is vertical in all patterns); (c) stress−strain curve for N330 including corresponding 2D WAXS patterns at specific strains between 100 and 400%.

particle size may create ideal conditions for SIC within the rubber matrix.

From the 1D WAXS profiles, the crystallite size and crystallinity of the composites and unfilled NR at 400% strain can be obtained. The crystallinity, χ, can be estimated from eq 1

$$\chi = \frac{I_c}{I_a + I_c} \times 100 \tag{1}$$

where I_c and I_a are the crystalline and amorphous integrated intensities respectively, which are obtained from fitting Gaussian functions to the (200), (120) peaks and amorphous halo (an example fit for NR/330 is shown in the Supporting Information Figure S6). To estimate the crystallite size, the Scherrer equation was used, eq 2

$$L_{(hkl)} = \frac{K\lambda}{\beta \cos \theta} \tag{2}$$

where $L_{(hkl)}$ is the crystallite size normal to the (200) and (120) diffraction planes, λ is the X-ray wavelength, θ is the Bragg angle, β is the full width at half-maximum (in radians) of the *hkl* plane and K is the constant 0.94.[39] The crystallite size $L_{(200)}$ (lateral width) and $L_{(120)}$ (breadth) of the crystallites and crystallinity at 400% strain,[38,40,41] were determined for the NR/CB composites and unfilled NR sample and are given in Table 3.

From Table 3, it is clear that $L_{(200)}$ and $L_{(120)}$ tend to increase with CB filler size up to NR/330, but then fall as the CB size increases. However, in the unfilled NR, the lateral crystallite size is relatively large but the crystallinity is low. The decreased crystallite size in NR/CB composites compared with unfilled NR has been observed before[33,34] and is attributed to the chain immobilization and volume fraction reduction in rubber able to take part in crystallization (occluded rubber). Our observation that $L_{(200)}$ and $L_{(120)}$ are greatest for the NR/330 composite is interesting as it correlates to the X-ray data show in Figures 4 and 5. Thus, we show that the NR/330 composite exhibits both the earliest onset of SIC and the greatest crystallite dimensions. Tantalisingly, from the X-ray data, this may show that the NR/330 composite represents the *sweet-spot* for inducing SIC in these NR/CB composites.

In summary, tensile testing was employed to evaluate the self-healing performance of the NR/CB system from a macroscopic performance perspective. WAXS results were utilized to elucidate the reinforcement effects of different CB particles from the perspective of SIC. However, the correspondence between the self-healing behavior and microstructural evolution remains unclear. In the following section, coupling FT rheology and LAOS analysis, we will be able to distinguish the distinct contributions of the polymer network and filler network to the self-healing performance.

Microscale Mechanism of Self-Healing. The filler dispersion and filler−filler interactions are further quantively characterized by the filler network strength response to repetitive low-strain deformation, i.e. Payne effect.[42] The Payne effect is caused by the disruption of the filler network and the release of the rubber trapped in the filler network under

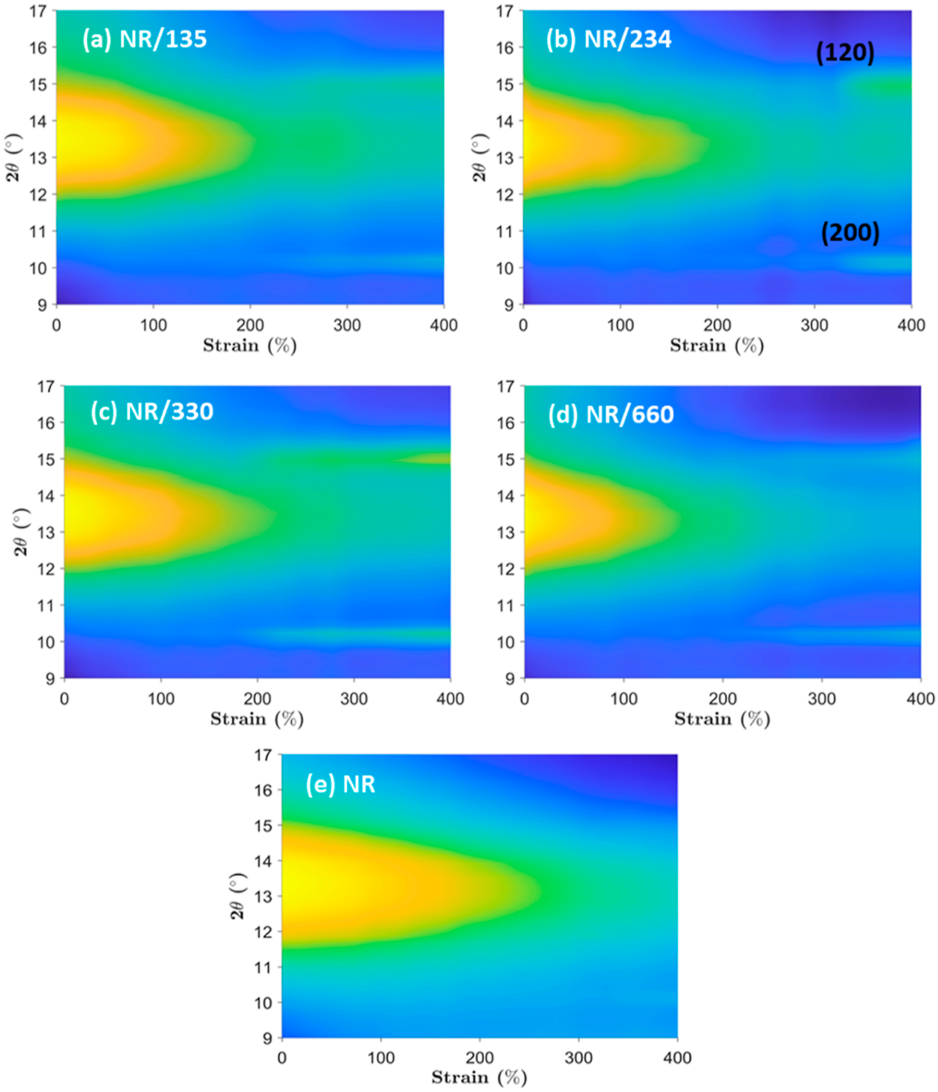

Figure 4. Surface plots showing equatorial scattering intensity for the WAXS data during the drawing of NR/CB composites and unfilled rubber. Each plot is shown over the 2θ region of 9−17° and from 0 to 400% strain. (a) NR/135, (b) NR/234, (c) NR/330, (d) NR/660, and (e) unfilled NR rubber.

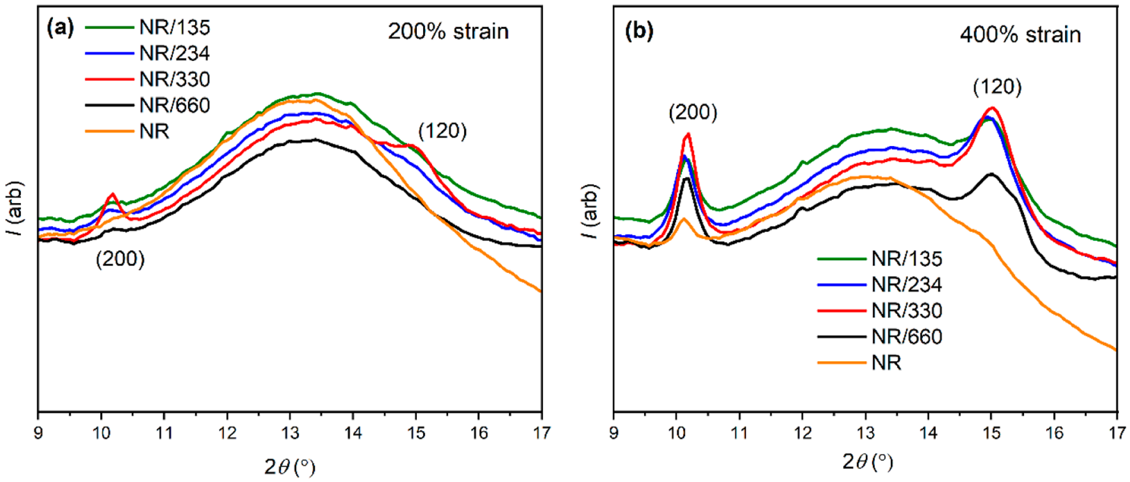

Figure 5. 1D WAXS profiles of NR/CB compounds at (a) 200% strain and (b) 400% strain showing the development of the (200) and (120) crystalline peaks.

https://doi.org/10.1021/acssuschemeng.3c06752
ACS Sustainable Chem. Eng. XXXX, XXX, XXX−XXX

Table 3. Estimated Crystallite Sizes from the (200) and (120) Peaks and Crystallinity of the NR/CB Composites and Unfilled NR Sample

	$L_{(200)}$ (Å)	$L_{(120)}$ (Å)	χ (%)
NR/135	111 ± 7	67 ± 4	21 ± 2
NR/234	110 ± 6	69 ± 4	24 ± 2
NR/330	136 ± 5	72 ± 3	24 ± 2
NR/660	82 ± 3	69 ± 4	21 ± 2
NR	124 ± 3		6 ± 1

oscillatory shear.[43] The low strain region reflects the filler−filler interactions, where the strain softening phenomenon is an indication of filler structure breakdown.

As shown in Figure 6a, the four NR/CB composites exhibit two obvious critical strain amplitude (γ_{c1}, γ_{c2}) for the onset of nonlinearity when approaching medium-amplitude oscillatory shear (MAOS) and large-amplitude oscillatory shear (LAOS) regimes. The γ_c is defined as the intersection of the extrapolation lines derived in different regimes. The storage modulus (G') for all the samples shows a plateau at $\gamma < \gamma_{c1}$, corresponding to the SAOS regime with plateau value of G_0'. The G_0' increases with the decrease of the CB size, indicating that smaller particles may form a stronger filler network. This is a consequence of being more homogeneously dispersed, the smaller particles with larger surface area can interact with more polymer chains at the interfaces, and trap "occluded rubber" inside the filler network. The constrained "occluded rubber" with reduced chain mobility yields a higher G_0' plateau value in the SAOS regime. In addition, the larger particles shift the γ_{c1} to a larger stain amplitude, showing a loosely interacted filler network and insensitivity to stress-softening as compared to the smaller fillers.

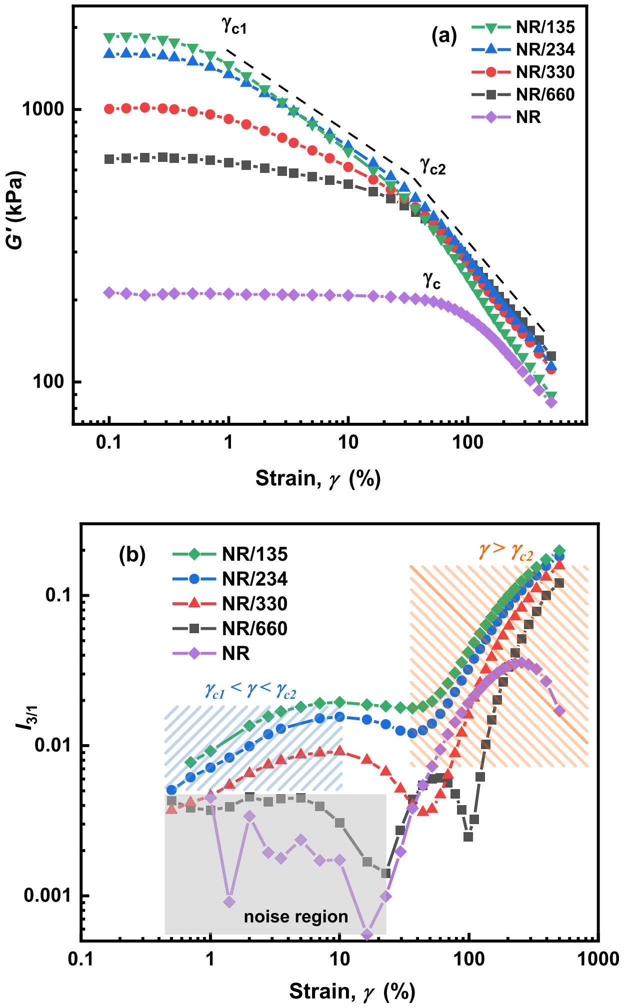

Figure 6. (a) Dependence of G' and G'' on the strain of cured NR and NR/CB compounds, (b) Normalized 3rd relative higher harmonics $I_{3/1}$ of the NR/CB composites of different CB.

When $\gamma > \gamma_{c1}$, G' drops drastically with strain, showing a typical strain-softening behavior. The discrepancy in $\Delta G'$ between strain (0.1−100%) of the four NR/CB (40 phr) samples was 374, 730, 1308, and 1602 kPa for the NR/660, NR/330, NR/234 and NR/135 composites, respectively; i.e., smaller particles induced larger strain-softening. Hence, the higher $\Delta G'$ value and narrower SAOS regime (earlier onset of the nonlinearity, or a smaller γ_{c1}) in the NR/CB composites, especially for NR/135, implying a stronger filler network and interfacial interactions.

Furthermore, it is noted that G' for all of the NR/CB composites crosses over at γ_{c2}, followed by a steeper decrease at larger strain amplitudes. In comparison, the unfilled NR shows one critical strain (γ_c) close to the γ_{c2} of the NR/CB. This phenomenon manifests that the second strain-softening of the NR/CB at $\gamma > \gamma_{c2}$ may be caused by the shear-induced change in the structure of the polymer network. The filler network was disrupted in the MAOS regime ($\gamma_{c1} < \gamma < \gamma_{c2}$) and the unfilled NR exhibits a similar strain-softening behavior at $\gamma_c \approx \gamma_{c2}$.

When large strain amplitudes are imposed, the stress response is no longer sinusoidal, and the LAOS stress data in the time domain can be analyzed through Fourier transform (FT) rheology. The quantification of rheological nonlinearity via FT-Rheology can be elucidated with a material under sinusoidal shear. The time-dependent strain for oscillatory shear experiments is given in a simplified complex notation, as shown in eq 3[44]

$$\gamma(t) = \gamma_0 e^{i(\omega_1 t)} \tag{3}$$

The stress response in the linear viscoelastic regime of the material can be described as a function of the modulus, as shown in eq 4[45]

$$\sigma(t) = G_0 \gamma_0 e^{i(\omega_1 t + \delta)} \tag{4}$$

with G_0 as the shear modulus at the excitation frequency and δ as the phase lag angle.

Once the material falls into the nonlinear viscoelastic regime, i.e., at LAOS where the structure of the material is changing during deformation, the stress response is still periodic but not sinusoidal anymore. The moduli G_0 in eq 4 can be described by the Taylor expansion series with even exponents[44]

$$\begin{aligned} \sigma(t) &= [G_1 + G_3\gamma(t)^2 + G_5\gamma(t)^4 + \ldots]\gamma_0 e^{i(\omega_1 t + \delta)} \\ &= \underbrace{G_1\gamma_0}_{I_1} e^{i(\omega_1 t + \delta)} + \underbrace{G_3\gamma_0^3}_{I_3} e^{i(3\omega_1 t + \delta_3)} \\ &\quad + \underbrace{G_5\gamma_0^5}_{I_5} e^{i(5\omega_1 t + \delta_5)} + \ldots \end{aligned} \tag{5}$$

The parameters G_1, G_3, G_5.... and δ_1, δ_2, δ_3..... are the prefactors and the phase angles of the Taylor series at the excitation frequency, third higher harmonic, fifth higher harmonics, and so on. FT of the stress in the time domain will consequently realize

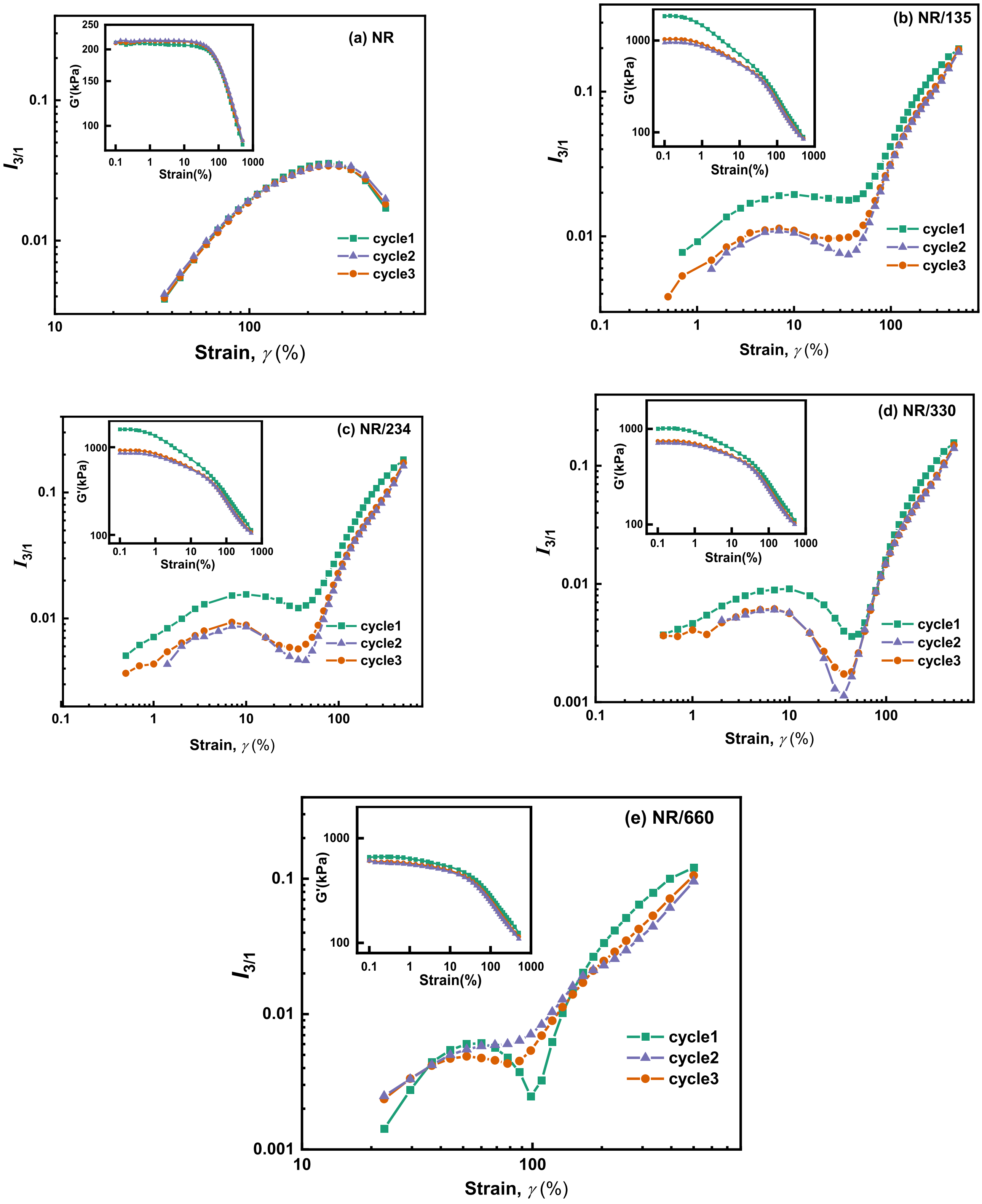

Figure 7. Evolution of $I_{3/1}$ of (a) NR, (b) NR/135, (c) NR/234, (d) NR/330, and (e) NR/660 composites for different healing cycles.

intensities (e.g., the absolute value of the parameters) at odd higher harmonics (ω_1, $3\omega_1$, $5\omega_1$, $n\omega_1$): I_1, I_3, I_5, I_n....., where n is an odd number. To compare the output signals from different experiments and samples to reduce experimental variations, the intensity at higher harmonics is normalized by the fundamental intensity I_1 giving the relative intensities, $I_{n/1}$[6]

$$I_{n/1} = I_n/I_1 \tag{6}$$

Among the relative intensities in the Fourier transformed spectra in the frequency domain, the third relative higher harmonic, $I_{3/1}$, is the highest and thus mostly used in FT-Rheology studies to quantify the nonlinearity.

$$I_{3/1} = \frac{I_3}{I_1} = \frac{G_3\gamma_0^3}{G_1\gamma_0} \tag{7}$$

Thereafter, this parameter is used as an indication of the nonlinear response. FT-rheology is particularly well-suited for complex polymer systems that exhibit a strong nonlinear viscoelastic behavior, where other conventional testing methods may not provide sufficient information. It is also coupled with the LAOS measurement to quantify the effect of dispersion and cross-linking on the final composites.[46−49] As such, normalized third relative intensities $I_{3/1}$ (γ_0) as a function of strain amplitudes (γ) were selected to probe the nonlinear rheological responses and displayed in Figure 6b.

Figure 6b shows $I_{3/1}-\gamma$ curves having distinct double-arc shapes with a local minimum around a strain amplitude of ≈51% (≈100% for NR/660). This is nearly equivalent to the strain amplitude where all of the G' (γ_0) from Figure 6a converged (γ_{c2}). In the corresponding MAOS and LAOS regions, $I_{3/1}$ increases with strain (γ) to different extents. Kádár et al.[50] observed similar plateau MAOS-LAOS transitions in their poly(ethylene-butyl acrylate) nanocomposite hybrids reinforced with graphite nanoplatelets and CB. They interpreted this plateau transition as an indication of a percolation threshold. Salehiyan and Hyun observed a similar double-arc shape in poly(lactic acid)/poly(caprolactone) blends filled with organoclays.[51] Their study revealed that adding clay to the blends resulted in increased compatibility and homogeneity, leading to a reduction in the strength of the local minimum, until it disappeared entirely. From Figure 6b, NR/CB with smaller sized CB has a higher $I_{3/1}$ value in both MAOS and LAOS regions, reflecting its higher nonlinearity generated by the stronger filler network.

After a continuous increase in the $I_{3/1}$ value in the MAOS region, the $I_{3/1}$ value levels off with a slight decay in a transition region (local minimum). The depth of this local minimum can further express the extent of separation between the two phases. The transition region (local plateau or local minimum ≈51%) for NR/135, NR/234 and NR/330 composites can be used to differentiate the two dominant MAOS and LAOS regions.

Different from these three composites, the NR/660 composite shows a gradual decrease in $I_{3/1}$ at the region of $\gamma_{c1} < \gamma < \gamma_{c2}$, instead of the initial obvious increase in $I_{3/1}$. This downward trend is more obvious in NR as shown in Figure 6b. In addition, both NR/660 and NR have lower $I_{3/1}$ values with fluctuation in this region compared to other NR/CB composites. The probable cause is equipment noise when the small torque response for NR/660 and NR in this region from the measurement is beyond the resolution of the torque transducer, which is also reported in other previous work.[1,44,50]

Note that NR/660 shows a much-delayed transition region at around 100% with a more pronounced local minimum (NR/660 ≈ 100%). The decreasing $I_{3/1}$ value and increasing local minimum with increasing CB particle size in NR/CB composites suggest weakening of the physical filler networks. The absence of the first arc-shape in the unfilled NR sample in the MAOS regime shows the absence of a filler network, i.e., this further confirms that the first nonlinear response in the MAOS regime is due to the filler network contribution.

To illustrate the role of the polymer network and filler network on the macroscale self-healing behavior of the composites, we tested the samples at strain amplitude (0.01−500%) and 60 °C, then subjected the samples to isothermal relaxation at 80 °C for 1 h; the same process was repeated twice to demonstrate the structural reversibility of the composites at the molecular level. Figure 7 compares the $I_{3/1}$ value with strain for different cycles, and the corresponding $G'-\gamma$ curves are also inserted.

From Figure 7a, the $G'-\gamma$ curves of the unfilled NR almost overlap each other over the three cycles, especially in the LAOS region $(\gamma > \sim 30\%)$. This rapid decrease of G' at large strain indicates the cross-linked rubber network might be deformed or ruptured, but the structure can be recovered or healed after the isothermal treatment at 80 °C for 1 h.

For the filled NR samples shown in Figure 7b−d, there is an obvious reduction in $I_{3/1}$ values at the MAOS region between cycles 1 and 2, and the curves nearly overlap during cycles 2 and cycle 3. This reveals that the physical CB filler network is disrupted in the MAOS regime during the first cycle and it is not recovered after the isothermal treatment at 80 °C.

In the LAOS regime, the $I_{3/1}-\gamma$ curves of the NR/330 composite are almost overlapped for the three cycles. The NR/234 and NR/135 containing smaller CB particles showed a reduction in their intensities after annealing at 80 °C in the LAOS region. As discussed above, this reflects that the filler networks formed by the smaller CB particles are disrupted after the first LAOS treatment; the overlapped second and third curves with lower $I_{3/1}$ intensities are due to the polymer network recovery. The NR/660 is the least affected in both MAOS or LAOS regions, as shown in Figure 7e, as discussed above; this may reflect a loose filler network formed by the large CB particles. The filler network strength and the filler−polymer interactions can be further quantified by the dynamic cross-link density (V_d) as determined by DMTA, the results are shown in Figure 8.

Figure 8 displays the dynamic temperature sweep test measured by DMTA at 1 Hz and 0.5% strain. The occurrence of the tan δ peak is closely related to the glass transition of the rubber chains. As derived from Figure 8a, the tan δ values at the peak are 1.65, 1.56, 1.26, and 1.11 for NR/660, NR/330, NR/234 and NR/135, respectively. The declining trend of the tan δ value in the NR/CB composites is caused by the different affinity between NR chains and CB fillers. The N135 CB with the largest surface area can interact with more rubber chains or trap more rubber in the CB filler network. The number of rubber chains that can participate in the glass transition would be highly reduced, thus resulting in a decreased tan δ.[28]

The glass transition temperature (T_g) obtained at the tan δ peak maximum shows a similar dependence on the CB surface area, see Table S3. The corresponding storage modulus variation with temperature is displayed in Figure 8b. The dynamic cross-link density (V_d) of NR/CB compounds can be calculated by eq 8[52]

$$V_d = \frac{E_r}{3RT} \tag{8}$$

where R refers to the universal gas constant while T is the absolute temperature, and E_r is the storage modulus in the rubbery plateau region $(T_g + 40\ °C)$.

As listed in Table S3, the V_d values of NR/CB composites increased from 7.55×10^{-4} to 1.588×10^{-3} mol/cm^3 with the decrease in CB particle size. Compared with the cross-link density (V_e) results determined by solvent equilibrium swelling (Table S2), the dynamic cross-link density V_d is higher than V_e by one to 2 orders of magnitude, and the V_d dependence on CB filler size is different from that of V_e, where the NR/234 has the highest V_e value. This difference is due to the different testing

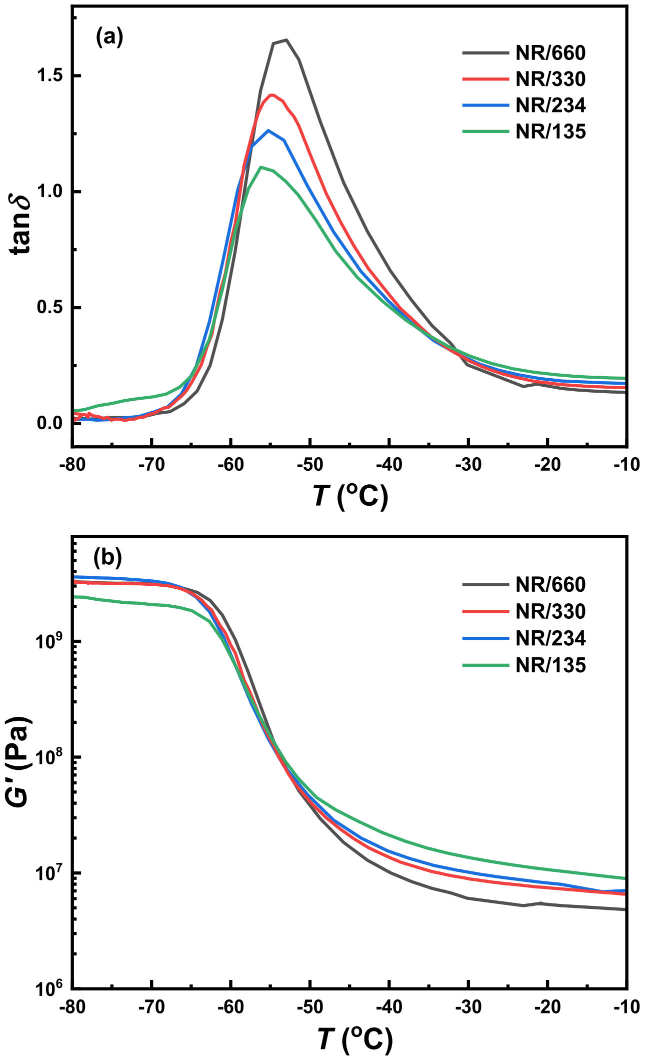

Figure 8. (a) Loss factor (tan δ) and (b) storage modulus (G') variation with temperature of cured NR/CB compounds measured by dynamic temperature sweep test at 1 Hz and 0.5% strain.

principles. The swelling method provides information about the cross-link density of the rubber matrix, while the V_d determined by DMTA reflects the overall viscoelastic contributions of both rubber and filler networks. Therefore, the V_d values are higher than V_e, and it is reasonable to interpret the polymer−polymer, polymer−filler, and filler−filler networks by considering the FT-rheology results and V_d.

As shown in Figure 9, the lowest V_d value for NR/660 verifies the least cross-link formation due to the smallest specific surface area of the N660 filler. Referring to Figure 7e, the least affected $I_{3/1}$ in MAOS and LAOS regions during shearing and self-healing processes is mainly ascribed to the inability to form a well-developed filler network. The NR/135 composite with the highest V_d and the lowest V_e values demonstrates an extensive involvement of the smallest CB particles in the formation of the cross-link networks in the NR/135 composites. Therefore, the coupling of FT-rheology and LAOS analysis has differentiated the contributions of the filler network and polymer network on the self-healing properties of the composites. The investigation of filler size in conventional vulcanized NR provides direct insight toward the sustainability of industrial rubber products from the perspectives of self-healing and reprocessability.

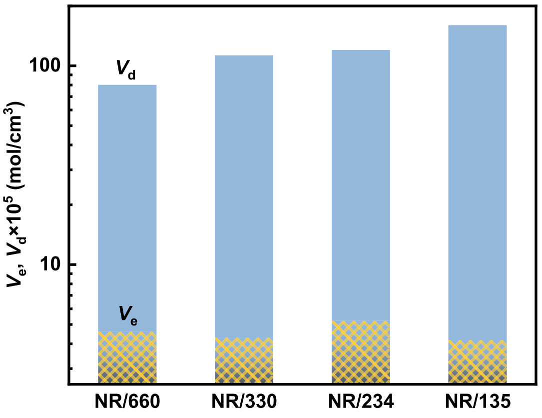

Figure 9. Comparison between V_e and V_d measured by the swelling method and DMTA, respectively.

In summary, utilizing research on self-healing and reprocessability in the development of sustainable rubber composite formulations holds immense potential for expanding the practical applications of these materials while promoting recycling and reusability without compromising stability and integrity. Specifically, the conditions simulated in large amplitude oscillatory shear (LAOS) experiments mirror the high shear rates and large deformations inherent in mechanical recycling processes. This approach offers a unique opportunity to design materials that retain their structural and mechanical integrity even after multiple recycling cycles. The insights derived from subjecting these materials to conditions mimicking real-world recycling processes provide invaluable data for engineering materials capable of enduring such rigorous treatments. Furthermore, exploring the behavior of these materials under multiple large deformations and subsequent healing processes becomes pivotal. Understanding the extent to which these materials maintain their properties posthealing, even after exposure to severe deformations, is crucial for ensuring their sustained utility across various industries. Industries involved in tire manufacturing, automotive components, construction materials, sealing materials, and any sector reliant on rubber-based products stand to benefit significantly from this approach. It opens doors to more sustainable practices by offering materials that not only possess self-healing capabilities but also endure repeated usage and recycling, contributing to a more ecofriendly and economically viable production cycle.

■ CONCLUSIONS

To understand the macroscale mechanical self-healing behavior, the microstructure recovery of NR/CB composites was quantitatively investigated by using FT-rheology coupled with LAOS across linear and nonlinear regimes (0.01−500%). The role of the CB particle size on the reinforcement and filler network recovery was discussed from the perspectives of filler dispersion, interfacial interaction, and SIC of NR.

For the four types of industrial grade CBs with particle size in the range of 20−50 nm, with 40 phr addition, they were all dispersed homogeneously in NR using a modified CV system. The NR/CB composites exhibit higher reinforcement effects and an earlier initiation of the SIC at 150−200% strain compared to NR. The large particle size (N660) showed higher mechanical self-healing efficiency, consistent with self-healing behavior revealed by LAOS cycles data measured by RPA.

Using FT-rheology and LAOS analysis, the relationship of the nonlinearity parameter $I_{3/1}$ as a function of strain amplitude was selected to probe the nonlinear rheological responses, where the roles of the filler−filler and polymer−polymer network can be differentiated. The nonlinear $I_{3/1}$ plots can be divided into two regions, where the filler network effect dominates the MAOS region, and the polymer networks dominate the LAOS region. The smaller fillers showed higher $I_{3/1}$ intensities and smaller local minimums, indicating a stronger filler network. It can be broken down during the first LAOS cycle, and the subsequent strain-softening behavior in the LAOS region is caused by the breakdown of the cross-linked polymer network. The structural recovery during the second and third cycles is mainly due to the polymer network self-healing via the reversible disulfide exchangeable bonds when treated at 80 °C, instead of filler network recovery. For the NR/660 composite, due to the lack of effective filler network formation, it presents similar viscoelastic behavior over the three cycles, i.e., the healing is mainly due to the polymer network recovery, therefore, it shows lower Payne effect and is less sensitive to the postprocessing conditions (i.e., healing). This work provides an efficient method to evaluate the self-healing and reprocessability of vulcanized rubbers from the microscale level, which complements their macroscale evaluation by conventional mechanical testing or repetitive compounding.

■ ASSOCIATED CONTENT

Data Availability Statement

The data sets generated during and/or analyzed during the current study are available from the corresponding author on reasonable request.

SI Supporting Information

The Supporting Information is available free of charge at https://pubs.acs.org/doi/10.1021/acssuschemeng.3c06752.

Experimental procedures, polymer characterization data, and data from our materials testing (PDF)

■ AUTHOR INFORMATION

Corresponding Author

Chaoying Wan − *International Institute for Nanocomposites Manufacturing (IINM), WMG, University of Warwick, Coventry CV4 7AL, U.K.;* orcid.org/0000-0002-1079-5885; Email: chaoying.wan@warwick.ac.uk

Authors

Tian Xia − *College of Material Science and Engineering, Chongqing University of Technology, Chongqing 400054, China; International Institute for Nanocomposites Manufacturing (IINM), WMG, University of Warwick, Coventry CV4 7AL, U.K.;* orcid.org/0000-0001-9468-8843

Alan M. Wemyss − *International Institute for Nanocomposites Manufacturing (IINM), WMG, University of Warwick, Coventry CV4 7AL, U.K.;* orcid.org/0000-0002-5919-9881

Reza Salehiyan − *International Institute for Nanocomposites Manufacturing (IINM), WMG, University of Warwick, Coventry CV4 7AL, U.K.; School of Computing, Engineering and the Built Environment, Edinburgh Napier University, Edinburgh EH10 5DT, U.K.*

Ellen L. Heeley − *School of Life, Health and Chemical Sciences, The Open University, Milton Keynes MK7 6AA, U.K.*

Xiao Hu − *International Institute for Nanocomposites Manufacturing (IINM), WMG, University of Warwick, Coventry CV4 7AL, U.K.*

Fengzai Tang − *WMG, University of Warwick, Coventry CV4 7AL, U.K.*

Yuchen Sun − *International Institute for Nanocomposites Manufacturing (IINM), WMG, University of Warwick, Coventry CV4 7AL, U.K.*

Darren J. Hughes − *WMG, University of Warwick, Coventry CV4 7AL, U.K.*

Tony McNally − *International Institute for Nanocomposites Manufacturing (IINM), WMG, University of Warwick, Coventry CV4 7AL, U.K.;* orcid.org/0000-0001-5436-4211

Complete contact information is available at: https://pubs.acs.org/10.1021/acssuschemeng.3c06752

Author Contributions

Tian Xia prepared materials and performed sample characterization, wrote and organized the main manuscript. Alan M. Wemyss carried out the initial experiments including tensile test, RPA, DMA, and WAXS. Reza Salehiyan analyzed the RPA data and wrote the LAOS discussion. Ellen L. Heeley and Darren J. Hughes wrote the WAXS data discussion. Xiao Hu and Fengzai Tang carried out the TEM experiment. Yuchen Sun verified the mechanical properties. Tony McNally revised the manuscript. Chaoying Wan initiated the concept and revised the manuscript. All authors reviewed the manuscript.

Funding

We gratefully acknowledge the research facility support from the WMG High-Value Manufacturing Catapult Centre. X-ray beamtime at the ESRF was provided under the experimental application 28-1-1262. XMaS is a UK national research facility supported by EPSRC. We are grateful for the assistance of all the XMaS beamline staff, in particular the local contact Oier Bikondoa. We are also grateful to the BM26 (DUBBLE) beamline for loan of instrumentation. We are grateful to Eleanor Crabb (OU) and Alistair Little (IINM) for X-ray data collection. Tian Xia acknowledges scholarship support from the China Scholarship Council (No. 202008500073) and thanks the IINM for hosting her research visit.

Notes

The authors declare no competing financial interest.

■ REFERENCES

(1) Nie, S.; Lacayo-Pineda, J.; Willenbacher, N.; Wilhelm, M. Aging of natural rubber studied via Fourier-transform rheology and double quantum NMR to correlate local chain dynamics with macroscopic mechanical response. *Polymer* **2019**, *181*, 121804.

(2) Leblanc, J. L. Investigating the Non-Linear Viscoelastic Behavior of Filled Rubber Compounds Through Fourier Transform Rheometry. *Rubber Chem. Technol.* **2005**, *78* (1), 54−75.

(3) Leblanc, J. L. Fourier transform rheometry on carbon black filled polybutadiene compounds. *J. Appl. Polym. Sci.* **2006**, *100* (6), 5102−5118.

(4) Leblanc, J. L. Effect of temperature on dynamic rheological properties of uncured rubber materials in both the linear and the nonlinear viscoelastic domains. *J. Appl. Polym. Sci.* **2012**, *126* (2), 408−422.

(5) Leblanc, J. L. Large amplitude oscillatory shear experiments to investigate the nonlinear viscoelastic properties of highly loaded carbon black rubber compounds without curatives. *J. Appl. Polym. Sci.* **2008**, *109* (2), 1271−1293.

(6) Nie, S.; Lacayo-Pineda, J.; Wilhelm, M. Fourier-transform rheology of unvulcanized styrene butadiene rubber filled with increasingly silanized silica. *Soft Mater.* **2019**, *17* (3), 269−282.

(7) Yan, P.; Zhao, W.; Zhang, B.; Jiang, L.; Petcher, S.; Smith, J. A.; Parker, D. J.; Cooper, A. I.; Lei, J.; Hasell, T. Inverse Vulcanized Polymers with Shape Memory, Enhanced Mechanical Properties, and Vitrimer Behavior. *Angew. Chem., Int. Ed.* **2020**, *59* (32), 13371−13378.

(8) Polgar, L.; Van Duin, M.; Broekhuis, A.; Picchioni, F. Use of Diels−Alder chemistry for thermoreversible cross-linking of rubbers: the next step toward recycling of rubber products? *Macromolecules* **2015**, *48* (19), 7096−7105.

(9) Imbernon, L.; Oikonomou, E.; Norvez, S.; Leibler, L. Chemically crosslinked yet reprocessable epoxidized natural rubber via thermo-activated disulfide rearrangements. *Polym. Chem.* **2015**, *6* (23), 4271−4278.

(10) Wei, H.; Yang, Y.; Huang, X.; Zhu, Y.; Wang, H.; Huang, G.; Wu, J. Transparent, robust, water-resistant and high-barrier self-healing elastomers reinforced with dynamic supramolecular nanosheets with switchable interfacial connections. *J. Mater. Chem. A* **2020**, *8* (18), 9013−9020.

(11) Du, W.; Jin, Y.; Shi, L.; Shen, Y.; Lai, S.; Zhou, Y. NIR-light-induced thermoset shape memory polyurethane composites with self-healing and recyclable functionalities. *Composites, Part B* **2020**, *195*, 108092.

(12) Guo, Z.; Bao, C.; Wang, X.; Lu, X.; Sun, H.; Li, X.; Li, J.; Sun, J. Room-temperature healable, recyclable and mechanically super-strong poly (urea-urethane) s cross-linked with nitrogen-coordinated boroxines. *J. Mater. Chem. A* **2021**, *9* (17), 11025−11032.

(13) Yang, F.; Pan, L.; Ma, Z.; Lou, Y.; Li, Y.; Li, Y. Highly elastic, strong, and reprocessable cross-linked polyolefin elastomers enabled by boronic ester bonds. *Polym. Chem.* **2020**, *11* (19), 3285−3295.

(14) Lei, Z. Q.; Xie, P.; Rong, M. Z.; Zhang, M. Q. Catalyst-free dynamic exchange of aromatic Schiff base bonds and its application to self-healing and remolding of crosslinked polymers. *J. Mater. Chem. A* **2015**, *3* (39), 19662−19668.

(15) Efstathiou, S.; Wemyss, A. M.; Patias, G.; Al-Shok, L.; Grypioti, M.; Coursari, D.; Ma, C.; Atkins, C. J.; Shegiwal, A.; Wan, C.; Haddleton, D. M. Self-healing and mechanical performance of dynamic glycol chitosan hydrogel nanocomposites. *J, Mater. Chem. B* **2021**, *9* (3), 809−823.

(16) Wemyss, A. M.; Bowen, C.; Plesse, C.; Vancaeyzeele, C.; Nguyen, G. T. M.; Vidal, F.; Wan, C. Dynamic crosslinked rubbers for a green future: A material perspective. *Mater. Sci. Eng. R Rep.* **2020**, *141*, 100561.

(17) Wemyss, A. M.; Ellingford, C.; Morishita, Y.; Bowen, C.; Wan, C. Dynamic Polymer Networks: A New Avenue towards Sustainable and Advanced Soft Machines. *Angew. Chem., Int. Ed.* **2021**, *60* (25), 13725−13736.

(18) Deng, X.-Y.; Xie, H.; Du, L.; Fan, C.-J.; Cheng, C.-Y.; Yang, K.-K.; Wang, Y.-Z. Polyurethane networks based on disulfide bonds: from tunable multi-shape memory effects to simultaneous self-healing. *Sci. China Mater.* **2019**, *62* (3), 437−447.

(19) An, S. Y.; Noh, S. M.; Nam, J. H.; Oh, J. K. Dual Sulfide-Disulfide Crosslinked Networks with Rapid and Room Temperature Self-Healability. *Macromol. Rapid Commun.* **2015**, *36* (13), 1255−1260.

(20) Hernández, M.; Grande, A. M.; Dierkes, W.; Bijleveld, J.; van der Zwaag, S.; García, S. J. Turning Vulcanized Natural Rubber into a Self-Healing Polymer: Effect of the Disulfide/Polysulfide Ratio. *ACS Sustainable Chem. Eng.* **2016**, *4* (10), 5776−5784.

(21) Gent, A.; Lai, S. M. Interfacial bonding, energy dissipation, and adhesion. *J. Polym. Sci., Part B: Polym. Phys.* **1994**, *32* (8), 1543−1555.

(22) Hernández, M.; Grande, A. M.; van der Zwaag, S.; García, S. Monitoring Network and Interfacial Healing Processes by Broadband Dielectric Spectroscopy: A Case Study on Natural Rubber. *ACS Appl. Mater. Interfaces* **2016**, *8* (16), 10647−10656.

(23) Lee, G.; Song, H. Y.; Choi, S.; Kim, C. B.; Hyun, K.; Ahn, S.-k. Harnessing β-Hydroxyl Groups in Poly(β-Amino Esters) toward Robust and Fast Reprocessing Covalent Adaptable Networks. *Macromolecules* **2022**, *55* (23), 10366−10376.

(24) Capelot, M.; Montarnal, D.; Tournilhac, F.; Leibler, L. Metal-Catalyzed Transesterification for Healing and Assembling of Thermosets. *J. Am. Chem. Soc.* **2012**, *134* (18), 7664−7667.

(25) Xu, Y.-z.; Fu, P.; Dai, S.-l.; Zhang, H.-b.; Bi, L.-w.; Jiang, J.-x.; Chen, Y.-x. Catalyst-free self-healing fully bio-based vitrimers derived from tung oil: Strong mechanical properties, shape memory, and recyclability. *Ind. Crop. Prod.* **2021**, *171*, 113978.

(26) Khimi, S.; Syamsinar, S.; Najwa, T. Effect of carbon black on self-healing efficiency of natural rubber. *Mater. Today Proc.* **2019**, *17*, 1064−1071.

(27) Utrera-Barrios, S.; Hernández Santana, M.; Verdejo, R.; López-Manchado, M. A. Design of rubber composites with autonomous self-healing capability. *ACS Omega* **2020**, *5* (4), 1902−1910.

(28) Wang, D.; Tang, Z.; Fang, S.; Wu, S.; Zeng, H.; Wang, A.; Guo, B. The use of inverse vulcanised polysulfide as an intelligent interfacial modifier in rubber/carbon black composites. *Carbon* **2021**, *184*, 409−417.

(29) Hu, X.; Zhang, R.; Wemyss, A. M.; Du, A.; Bao, X.; Geng, X.; Wan, C. Damping and electromechanical behavior of ionic-modified brominated poly (isobutylene-co-isoprene) rubber containing petroleum resin C5. *Ind. Eng. Chem. Res.* **2022**, *61* (8), 3063−3074.

(30) Basham, M.; Filik, J.; Wharmby, M. T.; Chang, P. C. Y.; El Kassaby, B.; Gerring, M.; Aishima, J.; Levik, K.; Pulford, B. C. A.; Sikharulidze, I.; Sneddon, D.; Webber, M.; Dhesi, S. S.; Maccherozzi, F.; Svensson, O.; Brockhauser, S.; Naray, G.; Ashton, A. W. Data Analysis WorkbeNch (DAWN). *J. Synchrotron Radiat.* **2015**, *22* (3), 853−858.

(31) Datta, R. *Rubber Curing Systems*; Flexsys, B.V., Ed.; Smithers Rapra Technology: *Shrewsbury*, 2002; Vol. *12*.

(32) Wemyss, A. M.; Marathianos, A.; Heeley, E. L.; Ekeocha, J.; Morishita, Y.; di Ronza, R.; Bernal, M. M.; Haddleton, D. M.; Wan, C. Oligomeric Curing Activators Enable Conventional Sulfur-Vulcanized Rubbers to Self-Heal. *ACS Appl. Polym. Mater.* **2022**, *4* (10), 7868−7877.

(33) Huneau, B. Strain-induced crystallization of natural rubber: a review of X-ray diffraction investigations. *Rubber Chem. Technol.* **2011**, *84* (3), 425−452.

(34) Poompradub, S.; Tosaka, M.; Kohjiya, S.; Ikeda, Y.; Toki, S.; Sics, I.; Hsiao, B. S. Mechanism of strain-induced crystallization in filled and unfilled natural rubber vulcanizates. *J. Appl. Phys.* **2005**, *97* (10), 103529.

(35) Bunn, C. W. Molecular structure and rubber-like elasticity I. The crystal structures of β gutta-percha, rubber and polychloroprene. *Proc. R. Soc. London, Ser. A* **1942**, *180* (980), 40−66.

(36) Toki, S.; Fujimaki, T.; Okuyama, M. Strain-induced crystallization of natural rubber as detected real-time by wide-angle X-ray diffraction technique. *Polymer* **2000**, *41* (14), 5423−5429.

(37) Toki, S.; Sics, I.; Ran, S.; Liu, L.; Hsiao, B. S.; Murakami, S.; Senoo, K.; Kohjiya, S. New Insights into Structural Development in Natural Rubber during Uniaxial Deformation by In Situ Synchrotron X-ray Diffraction. *Macromolecules* **2002**, *35* (17), 6578−6584.

(38) Beurrot-Borgarino, S.; Huneau, B.; Verron, E.; Rublon, P. Strain-induced crystallization of carbon black-filled natural rubber during fatigue measured by in situ synchrotron X-ray diffraction. *Int. J. Fatig.* **2013**, *47*, 1−7.

(39) InstaNANO. XRD Crystallite (grain) Size Calculator (Scherrer Equation). https://instanano.com/all/characterization/xrd/crystallite-size/, (accessed December 1, 2023)(12 April).

(40) Candau, N.; Laghmach, R.; Chazeau, L.; Chenal, J.-M.; Gauthier, C.; Biben, T.; Munch, E. Strain-Induced Crystallization of Natural Rubber and Cross-Link Densities Heterogeneities. *Macromolecules* **2014**, *47* (16), 5815−5824.

(41) Tosaka, M. Strain-Induced Crystallization of Crosslinked Natural Rubber As Revealed by X-ray Diffraction Using Synchrotron Radiation. *Polym. J.* **2007**, *39* (12), 1207−1220.

(42) Bokobza, L. The reinforcement of elastomeric networks by fillers. *Macromol. Mater. Eng.* **2004**, *289* (7), 607−621.

(43) Wang, M.-J. Effect of polymer-filler and filler-filler interactions on dynamic properties of filled vulcanizates. *Rubber Chem. Technol.* **1998**, *71* (3), 520−589.

(44) Cziep, M. A.; Abbasi, M.; Heck, M.; Arens, L.; Wilhelm, M. Effect of Molecular Weight, Polydispersity, and Monomer of Linear Homopolymer Melts on the Intrinsic Mechanical Nonlinearity 3Q0(ω) in MAOS. *Macromolecules* **2016**, *49* (9), 3566−3579.

(45) Dtsch, T.; Pollard, M.; Wilhelm, M. Kinetics of isothermal crystallization in isotactic polypropylene monitored with rheology and Fourier-transform rheology. *J. Phys.: Condens. Matter* **2003**, *15* (11), S923−S931.

(46) Kim, M.; Song, H. Y.; Choi, W. J.; Hyun, K. Evaluation of the Degree of Dispersion of Polymer Nanocomposites (PNCs) Using Nonlinear Rheological Properties by FT-Rheology. *Macromolecules* **2019**, *52* (22), 8604−8616.

(47) Salehiyan, R.; Song, H. Y.; Choi, W. J.; Hyun, K. Characterization of Effects of Silica Nanoparticles on (80/20) PP/PS Blends via Nonlinear Rheological Properties from Fourier Transform Rheology. *Macromolecules* **2015**, *48* (13), 4669−4679.

(48) Salehiyan, R.; Yoo, Y.; Choi, W. J.; Hyun, K. Characterization of Morphologies of Compatibilized Polypropylene/Polystyrene Blends with Nanoparticles via Nonlinear Rheological Properties from FT-Rheology. *Macromolecules* **2014**, *47* (12), 4066−4076.

(49) Salehiyan, R.; Song, H. Y.; Kim, M.; Choi, W. J.; Hyun, K. Morphological Evaluation of PP/PS Blends Filled with Different Types of Clays by Nonlinear Rheological Analysis. *Macromolecules* **2016**, *49* (8), 3148−3160.

(50) Kádár, R.; Abbasi, M.; Figuli, R.; Rigdahl, M.; Wilhelm, M. Linear and Nonlinear Rheology Combined with Dielectric Spectroscopy of Hybrid Polymer Nanocomposites for Semiconductive Applications. *Nanomaterials* **2017**, *7* (2), 23.

(51) Salehiyan, R.; Hyun, K. Effect of organoclay on non-linear rheological properties of poly(lactic acid)/poly(caprolactone) blends. *Korean J. Chem. Eng.* **2013**, *30* (5), 1013−1022.

(52) Yang, W.; Zhu, Y.; Liu, T.; Puglia, D.; Kenny, J. M.; Xu, P.; Zhang, R.; Ma, P. Multiple Structure Reconstruction by Dual Dynamic Crosslinking Strategy Inducing Self-Reinforcing and Toughening the Polyurethane/Nanocellulose Elastomers. *Adv. Funct. Mater.* **2023**, *33* (12), 2213294.